Available online at www.sciencedirect.com
ScienceDirect
Catalysis Today 131 (2008) 21–27
CATALYSIS TODAY
www.elsevier.com/locate/cattod

Use of Raman microscopy and band-target entropy minimization technique to differentiate physical mixture from chemical mixture in mixed metal oxides

Effendi Widjaja *, Jeyagowry T. Sampanthar *, Xuan Ding Han, Eunice Goh

*Institute of Chemical and Engineering Sciences, Agency for Science, Technology and Research (A*STAR), 1 Pesek Road, Jurong Island, Singapore 627833, Singapore*

Available online 3 December 2007

Abstract

Raman microscopy has been applied to characterize physical and chemical mixtures of mixed metal oxides. The obtained Raman mapping data were first subjected to singular value decomposition to obtain the right singular vectors, and the right singular vectors were then subjected to band-target entropy minimization (BTEM) to recover the pure component spectra of the observed species present in the sample. Subsequently, these resolved pure component spectral information was used to differentiate the physical and chemical mixtures. In addition, BTEM is also able to recover the pure component spectra of both unstable compound and its degradation product due to laser irradiation. In current study, the physical mixture of Mn_2O_3 and Co_3O_4, and the chemical mixture of $CoMn_2O_4$ spinel oxide were investigated.

Keywords: Raman microscopy; Band-target entropy minimization; Physical mixture; Chemical mixture; Mixed metal oxide; Raman bands

1. Introduction

Raman spectroscopy, which is one of the various analytical instruments used to characterize solid catalysts, is used to obtain the characteristics of the surface molecular structures. Raman spectroscopy has been applied to characterize various bulk and supported single and mixed metal oxides [1–10]. In situ Raman spectroscopy has also been applied to investigate the structural changes of metal oxides during transformations [11,12].

With the development of analytical instrumentation, an optical microscope can be attached to a Raman spectrometer to build a Raman microscopy. It is now possible to construct a Raman map containing both spectral and spatial information from a sample under characterization. This mapping measurement is performed by scanning in a grid pattern over the surface of the sample via programmed movements of a microscope objective. Therefore, using Raman microscopy will enable a user to examine the Raman band structures which are associated with chemical and structural properties of the investigated materials as well as the spatial distribution of materials in two spatial dimensions.

In current study, we attempted to develop an alternative method, which can be applied to differentiate between physical and chemical mixtures in the prepared mixed metal oxides. This method works by combining Raman mapping measurements with a multivariate data analysis technique, i.e. self-modeling curve resolution (SMCR) [13–16]. SMCR is a numerical technique specifically developed to resolve pure component spectra from a set of mixture spectra without any recourse to spectral library. The ultimate goal of SMCR is to determine the number of detected individual constituents, their identity, and their relative concentrations directly from the original data. When a Raman mapping data is analyzed, SMCR is also able to produce the spatial distribution of each component. Among all available SMCR techniques, band-target entropy minimization (BTEM) [17] is specifically developed to recover signals from trace components and to reconstruct the full-range pure component spectrum associated with a targeted spectral features. BTEM has been applied to a large variety of liquid-phase multi-component systems [18–20] as well as

* Corresponding authors. Fax: +65 6316 6185.
E-mail addresses: effendi_widjaja@ices.a-star.edu.sg (E. Widjaja), T_Jeyagowry@ices.a-star.edu.sg (J.T. Sampanthar).

0920-5861/$ – see front matter © 2007 Elsevier B.V. All rights reserved.
doi:10.1016/j.cattod.2007.10.079

solid-state chemical problems [21–23], and in current investigation BTEM was applied to analyze the Raman mapping data obtained from both physical and chemical mixtures of mixed metal oxides.

2. Experimental

2.1. Chemicals

All the chemicals and reagents, $Mn(CH_3COO)_2{\cdot}4H_2O$, $KMnO_4$, $Co(NO_3)_2{\cdot}4H_2O$, 37.5% HCl, used in the experiments, were analytically pure and were purchased from Sigma–Aldrich. They were used without any further purification. Mn_2O_3 and Co_3O_4 were obtained by calcinations of corresponding metal salts ($Mn(CH_3COO)_2{\cdot}4H_2O$ and $Co(NO_3)_2{\cdot}6H_2O$ at 550 °C in static air atmosphere. The XRD patterns confirmed the formation of pure phase of Mn_2O_3 and Co_3O_4.

2.2. Preparation of chemical mixture of mixed metal oxide—synthesis of spinel oxide of $CoMn_2O_4$

In a typical procedure, solutions of 0.5 M $KMnO_4$ and 0.5 M $Co(NO_3)_2$ were prepared separately by dissolving appropriate mass of chemicals with distilled water. 10.0 mL of 0.5 M $KMnO_4$ and 45 mL of 0.5 M $Co(NO_3)_2$ were mixed in a round bottom flask followed by dropwise addition of 1.0–1.5 mL HCl solution into the continuous stirring 1 M reaction mixture at room temperature until it reached the pH of 1. After the addition of HCl, the reaction mixture was then allowed to stir for 30 min at room temperature. The reaction mixture was later transferred into a Teflon-lined stainless-steel autoclave, which was sealed and maintained at about 200 °C, for various duration of time (1, 2, . . .,8 h), and after that it was cooled to room temperature. The suspension solution with fine precipitate was centrifuged and washed using distilled water until the pH was equal to 7. According to the XRD analysis, the aging time of 8 h formed a spinel oxide of $CoMn_2O_4$ (Fig. 1). The formation of spinel oxide occurred through hydrotalcites formation, which was further confirmed by the various aging time product analysis by XRD. Figs. 2 and 3 further verify the spinel oxide of $CoMn_2O_4$. Fig. 2 shows the XRD patterns of $CoMn_2O_4$ calcined in static air at temperatures of 450 and 650 °C. Fig. 3 shows the FE-SEM image of $CoMn_2O_4$.

2.3. Preparation of physical mixture of mixed metal oxide

A physical mixture was prepared by grinding and mixing pure Co_3O_4 with pure Mn_2O_3 with the composition ratio of 1:2 in a mortar.

2.4. Raman microscopy characterization

A thin layer of catalyst sample was prepared and put on the top of a microscope slide. Raman spectra were measured using a Raman microscope (In Via Reflex, Renishaw) equipped with deep-depleted thermoelectrically Peltier cooled CCD array

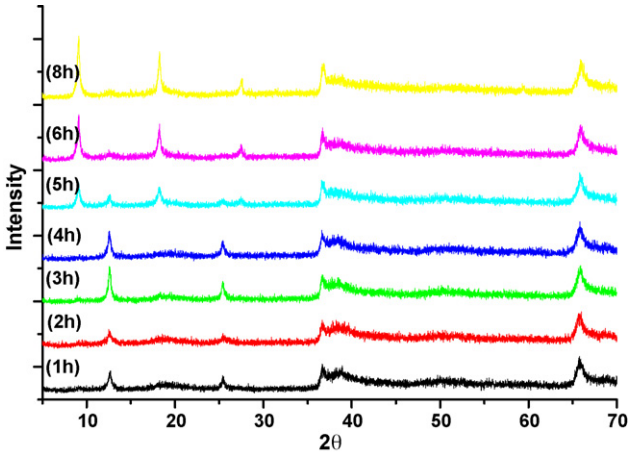

Fig. 1. The powder XRD pattern of the synthesized $CoMn_2O_4$ at various aging time. (At aging time from 1 to 4 h, products are in hydrotalcites form, at aging time 5 h, product shows mixture of hydrotalcites and spinel oxides form, and at aging time from 6 to 8 h, products already show the formation of spinel oxide form.)

detector (576 × 384 pixels) and a high grade Leica microscope. The Raman scattering was excited with a visible 514.5 nm argon ion laser and a 50× objective lens was used to collect the backscattered light. Raman point-by-point mapping with a step size of 20 μm in both the *x* and *y* directions was performed on the area of 100 μm × 100 μm. Scans were collected in an extended spectral window from 100 to 1200 cm^{-1} and the acquisition time for each spectrum collection was around 180 s. The final three-dimensional Raman imaging data cube collected from one experiment is of the format of 6 × 6 × 952.

2.5. Spectral preprocessing

The Raman mapping data is first reorganized from a three-way array to a conventional two-way array (pixel × channel) for processing. Since the raw Raman spectra acquired from physical and chemical mixtures were the combination of Raman scattering signals, spikes due to cosmic rays, and autofluorescence background, some spectral pre-processing was needed to generate Raman spectral alone. Spikes were removed in the first step followed by baseline correction

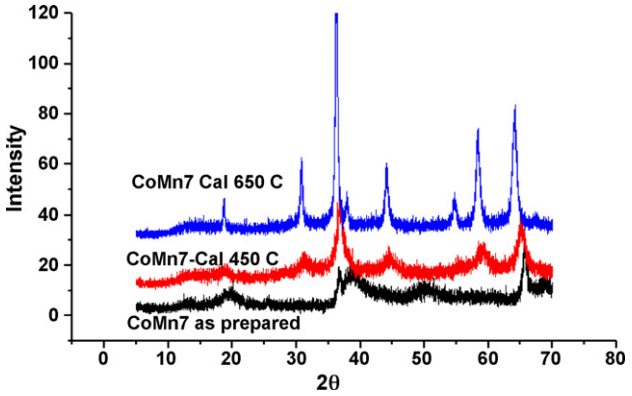

Fig. 2. The powder XRD pattern of $CoMn_2O_4$, which is calcined in static air at temperatures 450 and 650 °C.

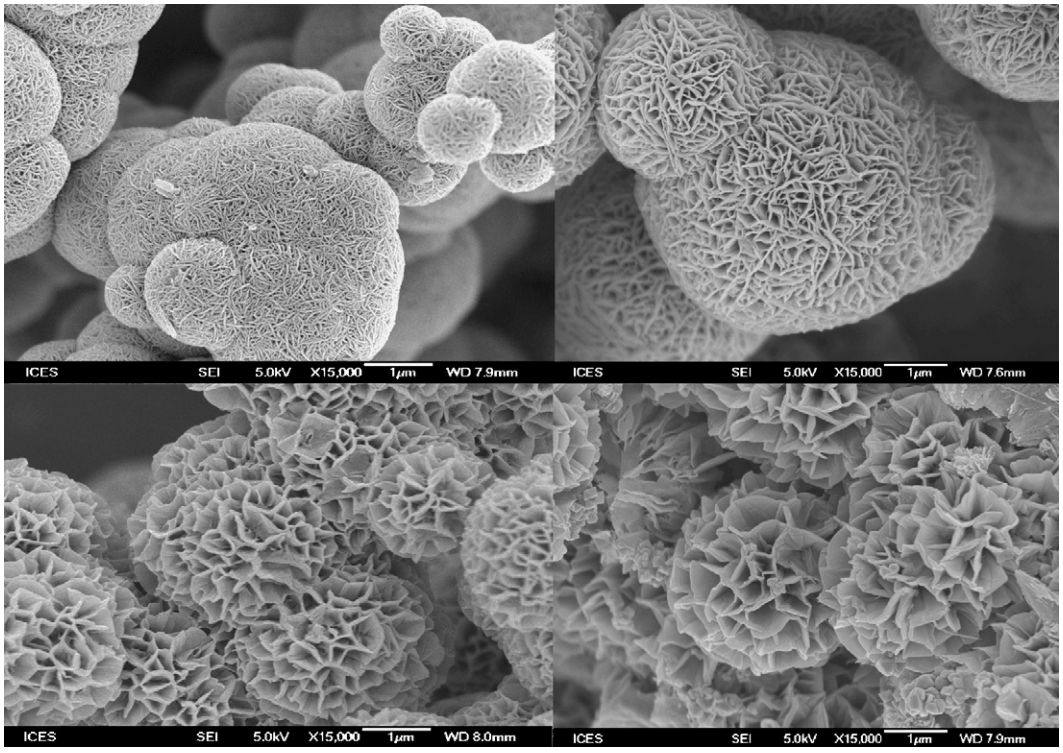

Fig. 3. The FE-SEM image of $CoMn_2O_4$ nanoflowers.

using second order modified polynomial fitting, and spectral normalization to unit height.

2.6. Band-target entropy minimization (BTEM)

The primary use of BTEM is to extract the pure component spectra from a set of multi-component mixture spectra. Subsequently, the contributions of each individual pure component spectrum to the sum-total measured experimental spectrum are back-calculated.

Let $\mathbf{I}_{k\times\nu}$ represent the Raman intensity in the consolidated spectroscopic data matrix where k denotes the number of spectra taken, and ν denotes the number of data channels associated with the spectroscopic range. The experimental intensities $\mathbf{I}_{k\times\nu}$ have a bilinear data structure and can be described as a product of two sub-matrices, namely, the concentration matrix $\mathbf{C}_{k\times s}$ and the Raman pure component scattering coefficient matrix $\mathbf{J}_{s\times\nu}$ (where s denotes number of observable species in the chemical mixture). Accordingly, the associated error matrix $\boldsymbol{\varepsilon}_{k\times\nu}$ contains both experimental error and model error (non-linearities) [24].

$$\mathbf{I}_{k\times\nu} = \mathbf{C}_{k\times s}\mathbf{J}_{s\times\nu} + \boldsymbol{\varepsilon}_{k\times\nu} \tag{1}$$

The BTEM algorithm proceeds by first decomposing $\mathbf{I}_{k\times\nu}$ into its singular vectors using singular value decomposition (SVD). This is then followed by the appropriate transformation of right singular vectors, $\mathbf{V}^{\mathrm{T}}$, into physically meaningful pure component spectra.

$$\mathbf{I}_{k\times\nu} = \mathbf{U}_{k\times k}\boldsymbol{\Sigma}_{k\times\nu}\mathbf{V}^{\mathrm{T}}_{\nu\times\nu} \tag{2}$$

Different from other SMCR methods, BTEM is uniquely developed to resolve one pure spectrum at a time. The number of right singular vectors, z, taken for inclusion in the transformation is usually much larger than s due to the non-linearities present (non-stationary spectral characteristics). The number z is usually determined by identifying the vectors which possess localized signals of clear physical significance and retaining these, while discarding the vectors that are more-or-less randomly distributed noise.

$$\widehat{\mathbf{J}}_{1\times\nu} = \mathbf{T}_{1\times z}\mathbf{V}^{\mathrm{T}}_{z\times\nu} \tag{3}$$

To extract a pure spectrum $\widehat{\mathbf{J}}_{1\times\nu}$, a selected band present in the first few $\mathbf{V}^{\mathrm{T}}$ vectors is targeted. The BTEM algorithm then retains this feature, and at the same time, returns an entire spectrum which has a minimum entropy. This routine is repeated for all important observable physical features in the selected $\mathbf{V}^{\mathrm{T}}$ vectors. A superset of reconstructed spectra are obtained and this set is reduced to eliminate redundancies. This results in an enumeration of all observable pure component spectra.

As part of the process, the resulting pure spectral patterns are returned in a normalized form. When all normed observable pure component spectra have been reconstructed, the relative concentration values are recovered by projection onto the original data set. The score images for each pure component that represent its distribution in one particular area can be obtained by folding back the two-way array data into three-way array data. For detailed descriptions of BTEM algorithm, readers can refer to Refs. [17–23].

3. Results and discussion

3.1. Physical mixture

A simulated physical mixture between Co_3O_4 and Mn_2O_3 was prepared to mimic the formation of physical mixture of mixed metal oxides during spinel oxide synthesis. Fig. 4a shows the visible image of physical mixture of Co_3O_4 and Mn_2O_3 in the measured area of 100 μm × 100 μm. The collected Raman mapping data were reorganized and were preprocessed as mentioned in the procedure above. The first 20 preprocessed Raman spectra were shown in Fig. 4b. Since M_2O_3 is unstable under the power of laser irradiation, laser power from the source was reduced by density filter. As the result, the laser power was ca. 0.2 mW on the sample. Due to low laser power and weak Raman scattering from the sample, low signal to noise ratio was expected as shown in Fig. 4b.

Singular value decomposition (SVD) was performed and the resulting first nine right singular vectors or basis vectors were shown in Fig. 5. These basis vectors contain abstract information on the pure component spectra of the observable components present in the system. These basis vectors are ordered according to their contribution to the total variance in the observations. Hence, the first few vectors are associated with the chemically significant information in the system, and the remaining vectors are primarily associated with the random instrumental and experimental error. As can be seen in Fig. 5, the first five vectors have very clear localized signals and little noise. The next two vectors still possess localized signals but considerably more noise. The eighth and the remaining vectors were essentially only white noise. Accordingly, seven basis vectors were used in the subsequent BTEM spectral reconstructions. Three primary spectral features seen in Fig. 5 at 690–693, 651–655, and 312–318 cm^{-1} were used as band-targets, and subsequently three pure component spectra, i.e. Co_3O_4, Mn_2O_3, and Mn_3O_4 were resolved, respectively, from the targeted features. The full-spectral range pure component spectral estimates are shown in Fig. 6.

These BTEM spectral estimates were then compared with the pure component spectra of Co_3O_4 and Mn_2O_3 measured independently (Fig. 7) before mixing them. As can be seen in Figs. 6 and 7, there is a good agreement between pure reference and pure component spectrum estimate of Co_3O_4. The only differences were the small insignificant peak shifting and lower signal to noise ratio in pure spectrum BTEM estimate of Co_3O_4.

As mentioned before, Mn_2O_3 is unstable under laser irradiation. Photon irradiation can cause a localized thermal hotspot and this can easily induce structural changes of the Mn_2O_3 to Mn_3O_4. Most literatures reported the spectral mixture of Mn_2O_3 and Mn_3O_4 as the pure spectrum of Mn_2O_3. Since contributions from these two species to the measured spectrum are not static under laser irradiation, this has caused various different reports of pure component spectrum of Mn_2O_3 [3,7,25]. Fig. 7 presents two so-called "pure spectrum" of Mn_2O_3 measured using two different laser powers, i.e., 0.2 and 0.4 mW. At higher laser power, two peaks at 653 and 700 cm^{-1} were emerged into one broadened band with peak position shifted to 648 cm^{-1} and one shoulder at 680 cm^{-1}. The other two smaller peaks at 197 and 314 cm^{-1} remained but with lower intensities. This resulting measurement at higher laser power indicated that there was Mn_3O_4 formation during spectral acquisition. When BTEM analysis was applied to the Raman mapping data of physical mixture of Co_3O_4 and Mn_2O_3, not only the pure component spectra of these two species were recovered, but the pure component spectrum of Mn_3O_4 (Fig. 6) was also resolved. Raman spectrum estimate of Mn_3O_4 obtained from BTEM shows the well-defined bands at 310, 365, and 653 cm^{-1}. The first two bands may correspond to the bending modes of Mn_3O_4, and the third band may correspond to the symmetric stretching of Mn–O lattice. The BTEM estimated Raman spectrum of Mn_3O_4 was in accordance with the Raman spectra reported in earlier works [3,7,25]. The BTEM estimated Raman spectrum of Mn_2O_3 was also quite similar with the pure reference spectrum of Mn_2O_3 measured under lower laser power. The only observed differences were insignificant small peak shifting at lower region (BTEM estimate was shifted to 198 and 315 cm^{-1}) and quite significant peak shifting at higher region (BTEM estimate was shifted to 658 and 695 cm^{-1}). The small peaks shifting at lower region were due to the higher signal to noise ratio in the recovered

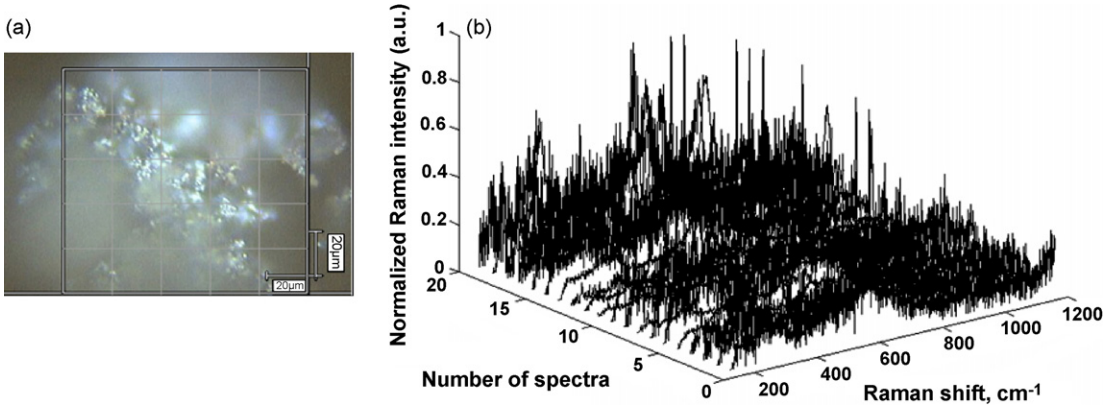

Fig. 4. (a) The visible image of physical mixture of Co_3O_4 and Mn_2O_3 in the measured area of 100 μm × 100 μm and (b) the first 20 preprocessed Raman spectra of physical mixture of Co_3O_4 and Mn_2O_3.

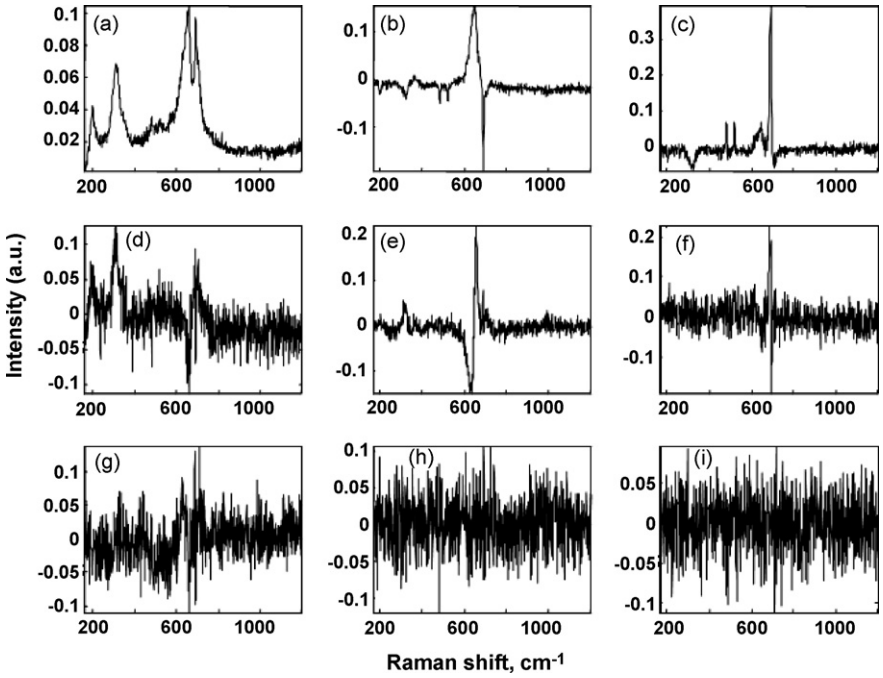

Fig. 5. The first nine right singular vectors of Raman mapping data of physical mixture of Co_3O_4 and Mn_2O_3: (a) first vector, (b) second vector, (c) third vector, (d) fourth vector, (e) fifth vector, (f) sixth vector, (g) seventh vector, (h) eighth vector, and (i) ninth vector.

Mn_2O_3 spectrum via BTEM. However, the more significant peak shifting at higher region (ca. 5 cm^{-1}) indicated that the measured Mn_2O_3 reference Raman signals under lower laser power was not only contributed from Mn_2O_3 species alone, but there were also small signal contributions from Mn_3O_4 species. Since Mn_2O_3 is unstable under laser irradiation, it is quite difficult to measure the pure Raman spectrum of this species without changing it to another structural form. However, as shown in this analysis, the pure component spectrum of Mn_2O_3 can still be determined by analyzing the Raman mapping data via BTEM method. The bands of BTEM estimated Mn_2O_3 at 198, 315, 658, and 695 cm^{-1} may correspond to the out-of-plane bending modes of Mn_2O_3 (first two bands) and the stretching modes of the Mn–O lattice (last two bands).

3.2. Chemical mixture

Fig. 8a shows the visible image of $CoMn_2O_4$ spinel oxide in the measured area of 100 μm × 100 μm. In order to prevent any structural transformation due to laser irradiation, very low laser power at ca. 0.06 mW was used to illuminate the measured sample. Similar to the abovementioned data analysis procedure, the collected Raman mapping data were reorganized and were preprocessed. The first 20 preprocessed Raman spectra were

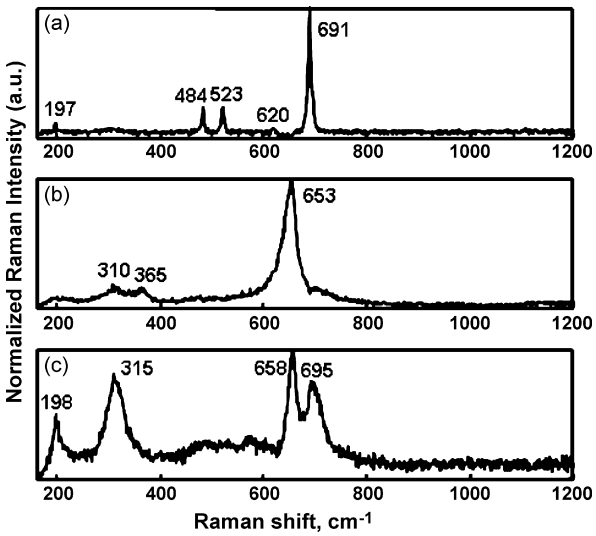

Fig. 6. Pure component Raman spectra estimates obtained via BTEM analysis: (a) Co_3O_4, (b) Mn_3O_4, and (c) Mn_2O_3.

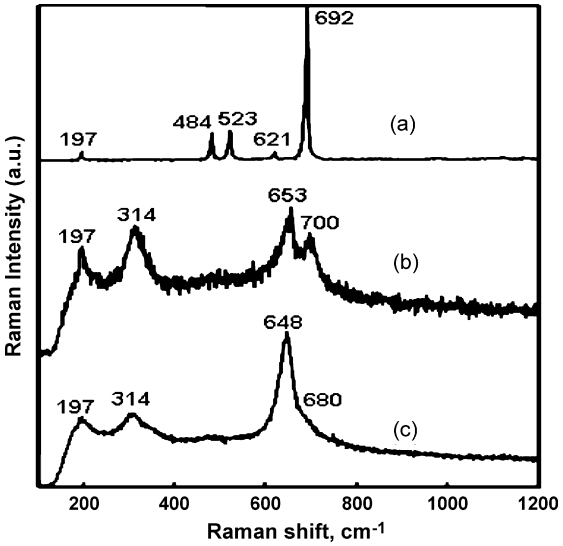

Fig. 7. Raman spectra of pure compounds: (a) Co_3O_4, (b) Mn_2O_3 measured using 0.2 mW laser power, and (c) Mn_2O_3 measured using 0.4 mW laser power.

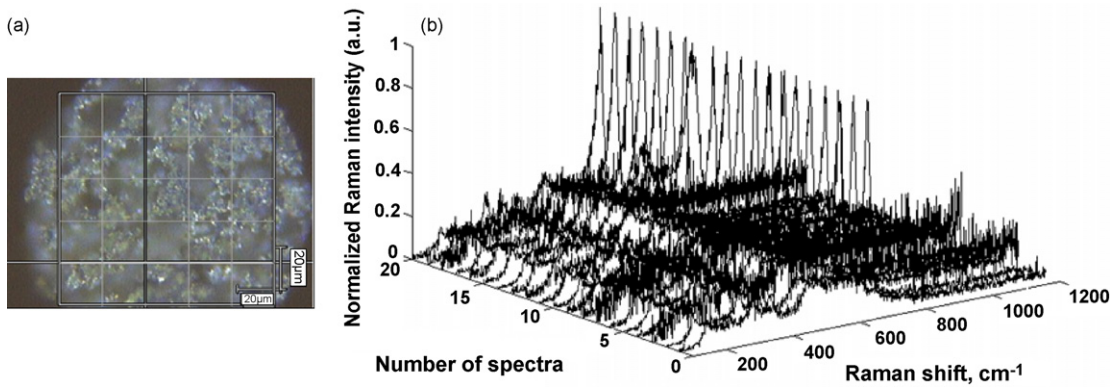

Fig. 8. (a) The visible image of $CoMn_2O_4$ spinel oxide in the measured area of 100 μm × 100 μm and (b) the first 20 preprocessed Raman spectra of chemical mixture of $CoMn_2O_4$ spinel oxide.

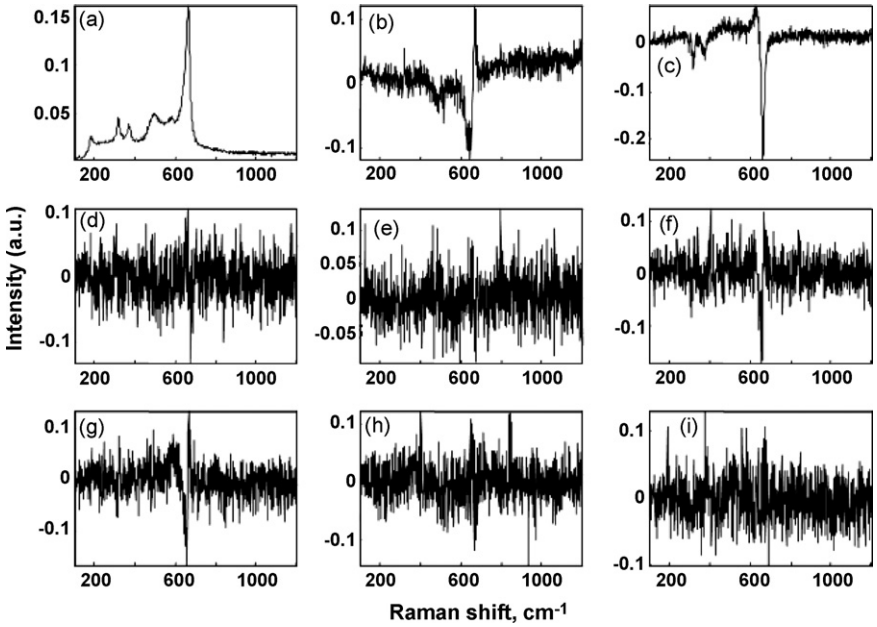

Fig. 9. The first nine right singular vectors of Raman mapping data of chemical mixture of $CoMn_2O_4$ spinel oxide: (a) first vector, (b) second vector, (c) third vector, (d) fourth vector, (e) fifth vector, (f) sixth vector, (g) seventh vector, (h) eighth vector, and (i) ninth vector.

shown in Fig. 8b. Again, SVD was performed on the 36 collected Raman spectra in order to generate the right singular vectors. As shown in Fig. 9, only the first three vectors have very clear localized signals and little noise. The remaining vectors were essentially noises. One prominent spectral feature at 662–665 cm^{-1} seen in the first three vectors was used as a band-target in the BTEM spectral reconstruction. Pure component spectrum of $CoMn_2O_4$ spinel oxide was then resolved accordingly and was shown in Fig. 10. Other spectral features at lower regions (200–600 cm^{-1} region) observed in the first and third vectors were also targeted. However, similar recovered spectral estimates of $CoMn_2O_4$ spinel oxide were obtained. Hence, based on the BTEM analysis result, it reconfirms the XRD characterizations that the synthesized spinel oxide is really a true chemical mixture. From Fig. 10, it is also shown that the Raman bands of $CoMn_2O_4$ spinel oxide are broader than that of Raman bands of Co_3O_4. With the incorporation of Mn into the lattice, the bands of Co_3O_4 are shifted, broadened, and some of them coalesce [26]. For instance, a pair of bands at 484 and 523 cm^{-1} in Co_3O_4 is coalesced to a single band at 495 cm^{-1} in $CoMn_2O_4$, the band at 197 cm^{-1} in Co_3O_4 is shifted to 180 cm^{-1} in $CoMn_2O_4$, and the band at 692 cm^{-1} in Co_3O_4 is now broadened and shifted to 664 cm^{-1} in $CoMn_2O_4$.

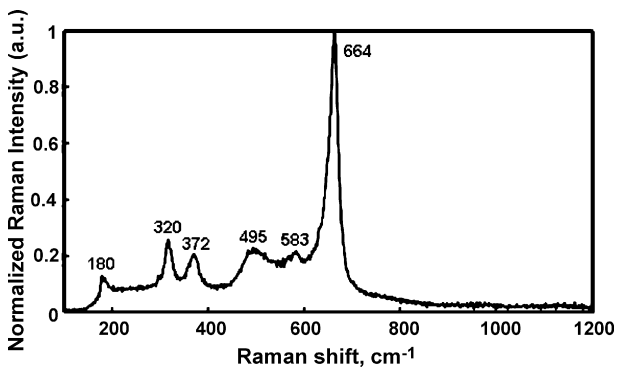

Fig. 10. Pure component Raman spectrum estimate of $CoMn_2O_4$ spinel oxide obtained via BTEM analysis.

4. Conclusions

From the two examples of Raman mapping measurements and BTEM analysis on physical and chemical mixed metal oxides, several conclusions can be drawn. First, the combined experimental and numerical technique provides an alternative tool to differentiate between physical and chemical mixtures of mixed metal oxide during the spinel oxide synthesis. When a true chemical mixture of spinel oxide is formed, BTEM analysis will recover only one pure component spectrum, which belongs to the spinel oxide itself. However, when a physical mixture is obtained during the synthesis, BTEM analysis will recover pure component spectra of several metal oxides used in the synthesis. In addition, the combined technique is also an efficient method to obtain the pure component spectra of a photo-sensitive or thermal sensitive sample. As laser irradiation could easily cause structural transformation in some metal oxides, it is difficult to measure the Raman pure component spectrum of original compound. However, using this technique, both the pure component spectra of original compound and product due to laser irradiation can be obtained.

References

[1] W. Li, G.V. Gibbs, S. Ted Oyama, J. Am. Chem. Soc. 120 (1998) 9041.
[2] F. Kapteijn, A.D. van Langeveld, J.A. Moulijn, A. Andreini, J. Catal. 150 (1994) 94.
[3] F. Buciuman, F. Patcas, R. Cracium, D.R.T. Zahn, Phys. Chem. Chem. Phys. 1 (1999) 185.
[4] R. Radhakrishnan, S.T. Oyama, J. Phys. Chem. B 105 (2001) 9067.
[5] M. Ferrandon, J. Carno, S. Jaras, E. Bjornbom, Appl. Catal. A: Gen. 180 (1999) 141.
[6] B.R. Strohmeier, D.M. Hercules, J. Phys. Chem. 88 (1984) 4922.
[7] M.-C. Bernard, A.H.-L. Goff, B. Vu Thi, J. Electrochem. Soc. 140 (1993) 3065.
[8] C. Julien, M. Massot, S. Rangan, M. Lemal, D. Guyomard, J. Raman Spectrosc. 33 (2002) 223.
[9] C. Julien, M. Massot, R. Baddour-Hadjean, S. Franger, S. Bach, J.P. Pereira-Ramos, Solid State Ionics 159 (2003) 345.
[10] C.V. Ramana, M. Massot, C.M. Julien, Surf. Interf. Anal. 37 (2005) 412.
[11] S.-C. Chang, M.A. Leugers, S.R. Bare, J. Phys. Chem. 96 (1992) 10358.
[12] D.Y. Lu, J. Chen, J. Zhou, S.Z. Deng, N.S. Xu, J.B. Xu, J. Raman Spectrosc. 32 (1996) 176.
[13] L.H. Lawton, E.A. Sylvestre, Technometrics 13 (1971) 617.
[14] B.M. Weckhuysen, A.A. Verberckmoes, A.R. De Baets, R.A. Schoonheydt, J. Catal. 166 (1997) 160.
[15] S. Sobanska, G. Falgayrac, J. Laureyns, C. Bremard, Spectrochim. Acta 64 (2006) 1102.
[16] Y. Batonneau, S. Sobanska, J. Laureyns, C. Bremard, Environ. Sci. Technol. 40 (2006) 1300.
[17] E. Widjaja, Development of band-target entropy minimization (BTEM) and associated software tools, PhD Thesis, National University of Singapore, 2002.
[18] E. Widjaja, C.Z. Li, W. Chew, M. Garland, Anal. Chem. 75 (2003) 4499.
[19] E. Widjaja, C.Z. Li, M. Garland, Organometallics 21 (2002) 1991.
[20] E. Widjaja, C.Z. Li, M. Garland, J. Catal. 223 (2004) 278.
[21] L.R. Ong, E. Widjaja, R. Stanforth, M. Garland, J. Raman Spectrosc. 34 (2003) 282.
[22] S.Y. Sin, E. Widjaja, L.E. Yu, M. Garland, J. Raman Spectrosc. 34 (2003) 795.
[23] E. Widjaja, N. Crane, T.–S. Chen, M.D. Morris, M.A. Ignelzi Jr., B.R. McCreadie, Appl. Spectrosc. 57 (2003) 1353.
[24] M. Garland, E. Visser, P. Terwiesch, D.W.T. Rippin, Anal. Chim. Acta 351 (1997) 337.
[25] C.M. Julien, M. Massot, C. Poinsignon, Spectrochim. Acta 60 (2004) 689.
[26] F. Kovanda, T. Rojka, J. Dobesova, V. Machovic, P. Bezdicka, L. Obalova, K. Jiratova, T. Grygar, J. Solid State Chem. 179 (2006) 812.